

# Experimental Investigation on Crushing of Granular Material in One-Dimensional Test

Yang Wu, Haruyuki Yamamoto, Akie Izumi

Received 04-03-2015, revised 27-05-2015, accepted 20-07-2015

## Abstract

A series of one-dimensional compression tests have been carried out on three kinds of granular materials in a dense state to investigate their mechanical and crushing behaviours. A new testing apparatus that can simultaneously measure the axial and lateral stresses acted on the cylindrical specimen was also developed. Experimental results show that the break-point stress on  $e - \log p$  curve is the largest for glass beads ballotini. A rise in compression index with the increasing axial load is observed for all three granular materials. The lateral earth pressure coefficient at rest  $K_o$  for the three granular materials slightly increases with the increasing axial load and attains a steady value between 0.25 and 0.3 at the initial loading stage. The value for  $K_o$  markedly increases as the axial load is removed during the unloading process. The axial strain of Masado is the largest at the same axial load level due to its mineral hardness. Experimental results demonstrate that the crushing degree of granular material is greatly influenced by the loading modes and conditions.

## Keywords

One-dimensional compression · particle crushing · grain size distribution · lateral earth pressure coefficient · compressibility

## Yang Wu

Department of Civil Engineering, Yamaguchi University, 2-16-1 Tokiwadai, Ube, Japan  
e-mail: yangwuuu0226@hotmail.com

## Haruyuki Yamamoto

Graduate School for International Development and Cooperation, Hiroshima University, 1-5-1 Kagamiyama, Higashi-Hiroshima, Japan  
e-mail: a040564@hiroshima-u.ac.jp

## Akie Izumi

Graduate School for International Development and Cooperation, Hiroshima University, 1-5-1 Kagamiyama, Higashi-Hiroshima, Japan

## 1 Introduction

In the last three decades, experimental study on particle crushing of granular material has attracted the attentions of many researchers [1–6]. Particle crushing is believed to be an irrecoverable process and sand grains are densified into a more compact state through inter-particle slip and rotation. Some engineering practise such as estimation of the bearing capacity of pile is greatly influenced by the variation in mechanical properties of sand in surrounding of pile tip due to particle crushing [7–10].

One-dimensional compression test is a common and effective measurement to examine the fundamental compression characteristics of granular material. These tests in literature are classified into two categories. One is to examine the effect of a specimen's physical properties on its compression behaviour. Hagerty *et al.* (1993) examined the effect of initial relative density, median grain size, particle shape and mineral components on different kinds of granular materials [11]. Nakata *et al.* (2001a, b) conducted plenty of one-dimensional compression tests on silica sand to examine the curvature and slope of the compression line, and the statistics of individual particle crushing in consideration of particle size and overall grading. The other one-dimensional tests aim to investigate the effect of the external experimental conditions [12, 13]. Graham *et al.* (2004) studied the compression properties of densely compacted sand with elevated temperature [14]. Yamamuro *et al.*, (1996), Wang and Wong (2010) reported the effect of time on the rate of particle crushing, respectively [15, 16]. Owing to the fully confined loading condition in one-dimensional compression, a variation in the lateral earth pressure coefficient  $K_o$  during one-dimensional loading-unloading tests has been discussed by many researchers [17–20]. The discrete element method provides the possibility of understanding the variation in the internal structure of assembled particles under compression and shear loadings [21–25].

However, the applied loading in previous one-dimensional testing is extremely high, therefore some individual grains are severely damaged [11]. Actually, particle crushing of most granular materials occur much earlier than the appearance of the break-point stress [12]. Therefore, the variation in the mechani-

cal properties of granular material under one-dimensional compression within such specific stress region should be furtherly investigated. This study presents a one-dimensional compression experimental study on two kinds of natural granular materials and one artificial granular material in a dense state under relatively high loading. The maximum load applied on the specimens composed of the same granular material is terminated at four levels in proportion to differentiate the occurrence of particle crushing and the variation in mechanical behaviour. The overall strength and deformation properties are represented and analyzed for each granular material. Variation in the lateral earth pressure coefficient during one-dimensional loading and unloading processes are demonstrated. Moreover, the effect of loading mode on degree of breakage is also confirmed in this study. Different breakage patterns for both natural and artificial granular materials are identified.

## 2 Testing Apparatus

The one-dimensional high pressure compression testing apparatus was composed of two half-part containments. Fig. 1(a) shows the side view of the one-dimensional testing apparatus. These two half-part containments were firmly fastened using four steel bars and sixteen screws to restrict lateral deformation of the specimen in cylinder cell. In practice, it was quite difficult to keep the radial strain as zero during the entire loading process. The opposite side of each steel bar is instrumented with a strain gauge so that lateral stresses on soil could be measured from the circumferential strains in the apparatus as shown in Fig. 1(b). The Young's modulus of the steel bar was approximately 210 GPa. Total lateral force acting on the specimen in the cylinder cell was expected to the summation of the tensile force on all steel bars. The radial stress is calculated as the ratio of measured summation force on steel bars by the sectional area of the specimen.

The internal cylinder cell for loading the sand specimen was 25.7 mm radius and 100 mm height. The diameter of axisymmetric specimen was 51.4 mm. The ratio of diameter to height for this apparatus is the same to the containment adopted by Yamamuro *et al.*, (1996) [15]. Three kinds of granular material specimens were prepared in the cylinder cell using the tamping method, with relative density  $Dr$  at 90% to examine the crushing behaviour at similar dense state. Slight height adjustment of the specimen for different granular material was made to achieve the desired relative density. Granular materials were poured into the cylinder cell by ten layers, densely tamped each time.

To eliminate the frictional stress generated on the internal surface of the testing apparatus, teflon sheets and silicon-grease were pasted on the interior surface of the cylinder cell. On the top and bottom surfaces of the specimen in cylinder cell, one cap and base steel stoppers were installed in advance of loading. Two load cells with maximum capacity measurement as 50 kN were installed on the top and bottom steel stoppers to estimate the average axial force acted on specimen. The decrement and

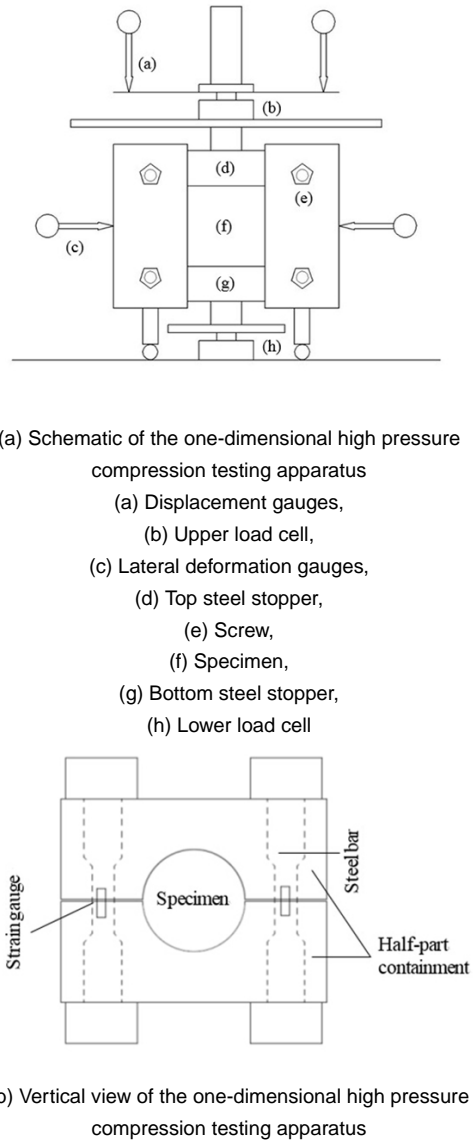


**Fig. 1.** Description of the one-dimensional high pressure compression testing apparatus

expansion of specimen in vertical and horizontal directions were recorded by the strain gauges on the steel plate and outer side wall of containment as shown in Fig. 2.

One-dimensional compression test was conducted on different specimens terminated at four maximum axial loads as 6 kN, 15 kN, 30 kN and 50 kN, respectively. All axial loads descend to the specimen at a constant rate of axial deformation as 0.02 mm/min. The unloading begins with a constant speed as 0.02 mm/min after the axial load attains the maximum value. Results of loading and deformation of specimens during loading-unloading process were recorded by a data-logger and computer during each loading-unloading process.

## 3 Tested Granular Materials

To clarify the mechanical behaviours of granular material in one-dimensional compression at relatively high pressure, three granular materials of different mineral components and hardness were used. The medium hardest, Toyoura sand, is a well graded

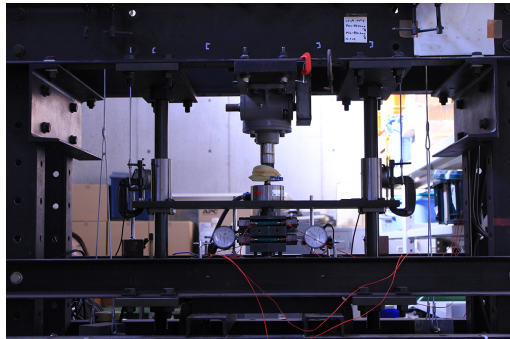


**Fig. 2.** Outline of one-dimensional high pressure compression testing apparatus

sand with particle size ranging from 0.074 mm to 0.5 mm, and with a maximum and minimum density of 1.646 g/cm<sup>3</sup> and 1.332 g/cm<sup>3</sup>. It is the standard sand recognized by Japan Geotechnical Society.

The softest granular material, Masado, is a kind of decomposed granite soil with grain size that ranges from 0.07 mm to 2 mm. Masado is distributed in large areas of land reclamation and coastal regions and the sample for this testing was taken from the region near Ota River in Hiroshima prefecture, Japan. Masado has also been employed in laboratory tests by many researchers [26–28].

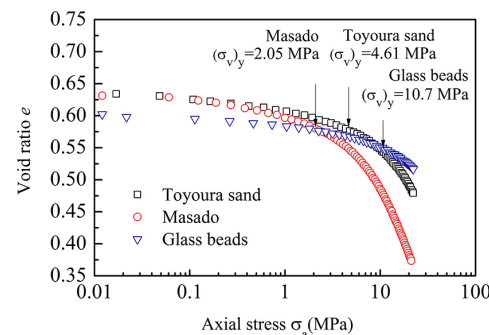
The hardest glass beads ballotini, are an assembly of the same size round particles and one kind of artificial plastic granular materials. Glass beads ballotini have an average diameter as 0.6 mm. Glass beads ballotini displays similar mechanical characteristics to brittle material and exhibits different breakage patterns in comparison with the natural sand. The physical properties for the Toyoura sand, Masado and glass beads ballotini are shown in Table 1.

#### 4 Test Results and Discussions

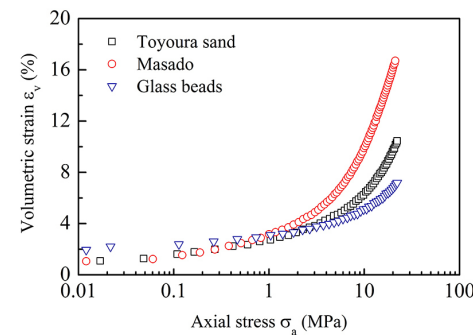
##### 4.1 Void ratio versus axial stress

Fig. 3 shows the void ratio versus the axial stress for three granular materials. The axial stress expressed in all figures represents an average load value measured by the two load cells on the specimen by the cross-sectional area of the specimen. Void ratio decreases gradually in the initial phase as the applied axial stress increases. The initial void ratios of Toyoura sand and Masado take almost the same values as 0.63, while that of glass beads ballotini is around 0.6. The maximum axial stresses acted on all three specimens are up to 22.5 MPa. As pointed out in previous studies [29, 30], the break-point on the curve after which the void ratio obviously reduces is identified for all three granular materials. The break-point corresponds to the point of maximum curvature on the  $e$ -log  $p$  curve. The break-point stress for the softest granular material in this test, Masado, is the smallest at 2 MPa. This is attributed to the wide distributed range of grain size and mineral hardness of Masado. Einav (2007) stated that larger particles get cushioned by surrounding smaller particles, making them more resistive to crushing, so that small particles

are more likely to be crushed [31]. The break-point stress for glass beads ballotini is largest at 10 MPa and it takes the value of 7 MPa for Toyoura sand. It can be thought that the break-point stress greatly depends on the mineral composition of the granular material.



**Fig. 3.** Void ratio versus axial stress for one-dimensional compression on three kinds of granular material



**Fig. 4.** Volumetric strain versus axial stress for one-dimensional compression on three kinds of granular material

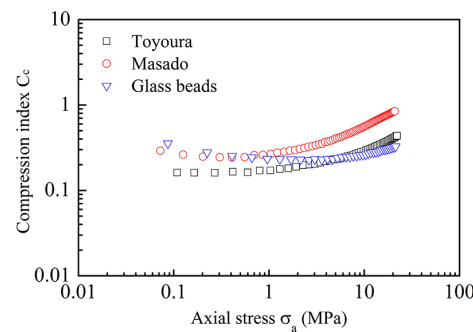


**Fig. 5.** Compression index versus axial stress for one-dimensional compression on three kinds of granular material

Three experimental curves express almost similar initial compressive behaviour when the axial stress is less than 1 MPa. The deformability and compressibility increase sharply once the axial stress exceeds the corresponding break-point stress for each granular material. The reducing ratio of  $e$ -log  $p$  curves for glass beads ballotini is relatively smaller compared with those of natural sand. It is due to the round shape and mineral composition of particle. Hagerty *et al.*, (1993) showed that there was a higher break-point stress for angular glass ballotini with the

**Tab. 1.** Physical parameters for the three kinds of granular materials

	Specific gravity (g/cm <sup>3</sup> )	Median diameter $d_{50}$ (mm)	Relative density (%)	Maximum density $\rho_{max}$ (g/cm <sup>3</sup> )	Minimum density $\rho_{min}$ (g/cm <sup>3</sup> )
Toyoura sand	2.656	0.195	90	1.646	1.332
Masado	2.648	0.676	90	1.641	1.347
Glass beads ballotini	2.595	0.602	90	1.608	1.428

same diameter size and pointed out that the angular glass ballotini displayed larger compressive behaviour in the early loading stage [11].

Fig. 4 represents a plot of volumetric strain against the logarithm axis of axial stress for three kinds of granular material. The volumetric strain  $\varepsilon_v$  is derived from  $\varepsilon_v = -\Delta e / (1 + e_0)$ . Herein,  $\Delta e$  and  $e_0$  are the void ratio variation and initial void ratio, respectively. It provides another approach to compare with the compressibility of these three granular materials. It is obvious that the volumetric strain significantly increases as the applied axial stress exceeds its corresponding break-point stress for each kind of granular material.

Fig. 5 represents the compression index  $C_c$  plotted versus the axial stress for Toyoura sand, Masado and glass beads ballotini, respectively. The compression index  $C_c$  is defined in Eq. (1) to quantify the compression degree of granular material under loading.

$$C_c = \frac{\delta e}{\delta \log(\sigma_a)} \quad (1)$$

where  $\sigma_a$  is applied axial stress. The compressibility of Toyoura sand slightly increases in the initial loading phase and becomes distinctively large as the axial stress goes beyond the break-point stress. The gradient is dependent on the curvature of the  $e$ -log  $p$  curve. The compression index is enlarged to almost five times of the initial value for Toyoura sand as the axial stress is elevated to 22.5 MPa. The compression index of Masado and glass beads ballotini initially decreases towards a steady value for a short time, before finally increasing. The reduction of the compression index in the beginning stage results from the rearrangement of particles and rotation of the glass beads.

#### 4.2 Axial stress-strain relationship

Figs. 6-8 display the axial stress plotted versus axial strain under loading-unloading for Toyoura sand, Masado and glass beads ballotini subjected to four maximum axial loads terminated at 6 kN, 15 kN, 30 kN and 50 kN, respectively. For the same granular material, the axial stress-strain curves at different axial loads show the similar shape and pattern. The critical state of specimen cannot be reached due to the ratio of applied axial stress to the radial stress is kept as a constant. It is observed that the increasing stiffness of tested granular materials in loading stage is due to the continual densification of granular material. It is noted that the initial slope of axial stress-strain curve for

each granular material expresses almost the same value and is less dependent on the final maximum terminated axial load.

The plots of axial stress against axial strain under one-dimensional loading-unloading for all three granular materials when the maximum axial stress is elevated to 22.5 MPa are shown in Fig. 9. Masado requires larger axial strain to reach the maximum axial stress. Simultaneously, it also displays significant irrecoverable axial strain compared with the other two kinds of granular materials when the unloading is finished. The irrecoverable axial strain is composed of the volumetric variation from the particle rearrangement and crushing.

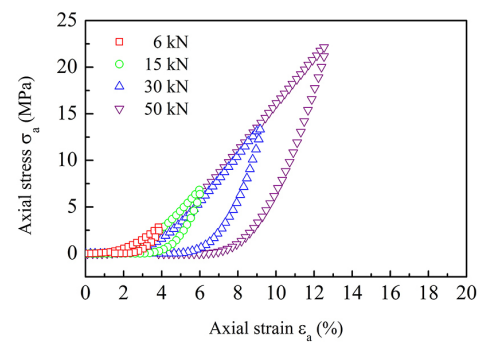


**Fig. 6.** Axial stress versus axial strain for one-dimensional compression test on Toyoura sand

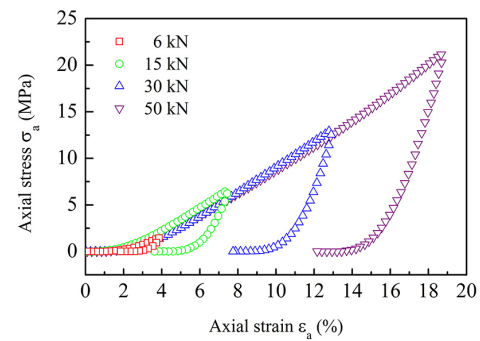


**Fig. 7.** Axial stress versus axial strain for one-dimensional compression test on Masado

The entire one-dimensional compression loading phase is divided into the primary compression part and secondary compression part by Mesri (2001) [32]. The dividing point was adopted by Hagerty et al., (1993) using the concept of crushing stress [11]. At stresses over the crushing stress, the addition of stress increment causes additional breakage and more obvious rearrangement of grains. It is specified that the slope of

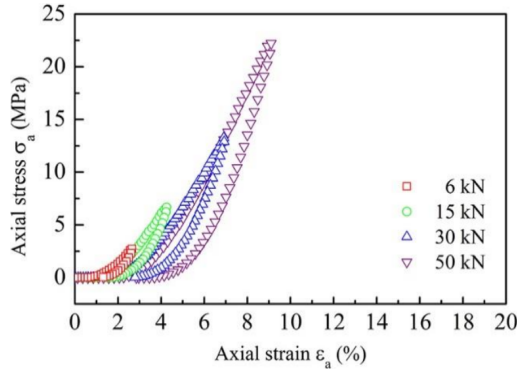


**Fig. 8.** Axial stress versus axial strain for one-dimensional compression test on glass beads ballotini

axial stress-strain curve increases rapidly once the applied axial stress is increased. Therefore, the volumetric behaviour in primary compression mainly comes from the compression of grains. The variation in volume in the secondary compression phase is the summary of the corresponding portions from compression and crushing. It is noted that the rate of axial stress to axial strain slightly increases and suddenly becomes steeper when axial stress is beyond the crushing stress during the loading process. As the axial stress reaches the maximum value and unloading begins, axial stress returns to zero again. The slopes of the stress-strain curve for the primary and secondary part of the loading phase as well as unloading phase are defined as the initial, secondary and unloading constrained modulus respectively, as shown in Fig. 10, respectively. The corresponding constrained modulus for the three kinds of granular material are shown in Table 2. Compared with the two natural sands, the initial constrained modulus of glass beads ballotini is lower. It is believed that the relative sliding and movement are easier for glass beads ballotini in comparison with natural sand in the primary compression phase. Therefore, the increment of axial strain is faster for glass beads specimens assembled with similar diameter-size ballotini. However, the secondary constrained modulus of glass beads ballotini is much higher than those of natural sands. In the secondary compression phase, the degree of crushing is relatively significant for natural sand due to a large volume of fines is produced in the loading phase. However, glass beads ballotini is only crushed into smaller fragments as the entire loading is applied. Test results demonstrate that the constrained modulus during unloading is less dependent on the mineral composition of granular material.

#### 4.3 Radial stress and axial stress

Figs. 11 - 13 represent the radial stress plotted against the axial stress for the three kinds of granular materials subjected to maximum axial load terminated at 6 kN, 15 kN, 30 kN and 50 kN, respectively. At different maximum loads, it is noted that the radial-axial stress curves express almost linearity for the three granular materials. Due to the specimen being prepared in a dense state, the radial stress appears instantly as the vertical stress acts on the specimen. The radial stress provided by the

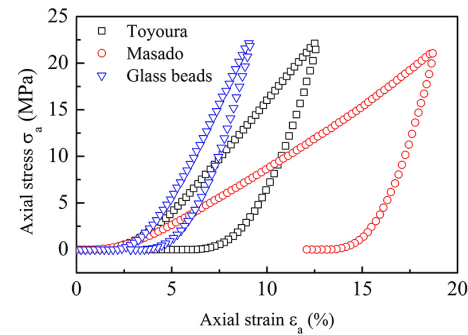


**Fig. 9.** Axial stress versus axial strain for three kinds of granular materials when maximum axial load is 50 kN

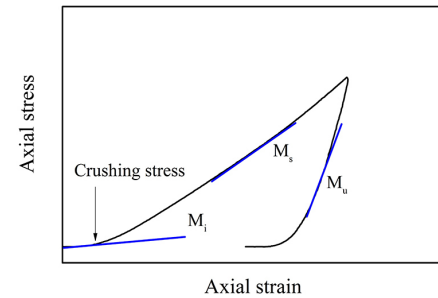


**Fig. 10.** Determination method of the initial, secondary and unloading constrained modulus for one-dimensional compression on granular material

interior surface of the containment cell increases in proportion to the increment of axial stress.

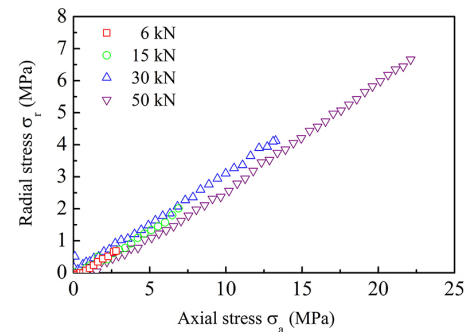


**Fig. 11.** Relationship between radial stress and axial stress for Toyoura sand

#### 4.4 $K_o$ in one-dimensional compression

The lateral earth pressure coefficient at rest  $K_o$  of three granular materials subjected to one-dimensional loading-unloading has also been investigated.  $K_o$  was defined by Bishop (1958) as the ratio of the lateral to vertical effective stresses in a consolidated soil under the condition of no lateral deformation [33]. It is also an important stress state in engineering design.  $K_o$  in loading process can be easily decided from the slope of radial-axial stress curve. Fig. 14 demonstrates that the curves for lateral earth pressure coefficient at rest plotted against the axial stress during loading process.  $K_o$  value attains 0.2 at low axial stress level and enters into a steady region with slight change as the axial stress is increased. The  $K_o$  at maximum axial stress level for

**Tab. 2.** Initial, secondary and unloading constrained modulus in loading-unloading process

	Initial constrained modulus $M_i$ (MPa)	Secondary constrained modulus $M_s$ (MPa)	Unloading constrained modulus $M_u$ (MPa)
Toyoura sand	3.491	252.091	701.376
Masado	2.028	139.199	712.686
Glass beads ballotini	0.766	402.104	680.726

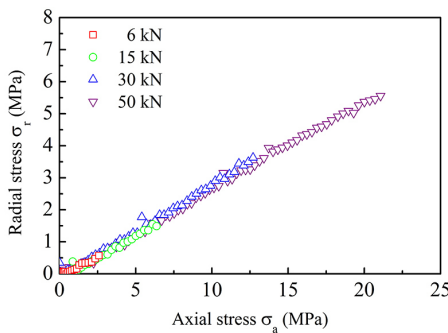


**Fig. 12.** Relationship between radial stress and axial stress for Masado

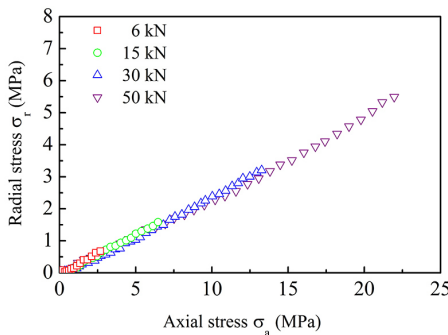


**Fig. 13.** Relationship between radial stress and axial stress for glass beads ballotini

Toyoura sand, Masado and glass beads ballotini are 0.29, 0.25 and 0.24, respectively. The differences are mainly originated from the different frictional angles of three granular materials.  $K_o$  value measured in this test is relatively smaller compared to the result reported by Yamamuro *et al.* (1996) [15]. It is believed that the axial stress acting on the specimen in that test is extremely high and causes significant particle crushing. The reduction of frictional angle after particle crushing makes the lateral earth pressure coefficient at rest increase.

The relationship between the axial stress and the lateral earth pressure coefficient  $K_o$  during unloading process are shown in Fig. 15. The lateral earth pressure coefficient at rest increases gradually from around 0.3 to 1.6 as the axial stress is reduced from the maximum value to zero. The experimental results by Gao and Wang (2014) also stated a similar variation tendency in the lateral earth pressure coefficient [34]. However, the final value for lateral earth pressure coefficient at rest when the unloading is completed in that test is larger than the results measured in our test because the applied maximum axial load is relatively high, approximately six or seven times of that in their test. The increasing  $K_o$  value during unloading results from radial

loading not fully recovering, even after unloading. The irrecoverable deformation causes part of the horizontal stress to remain locked in soil and destroys sand structure before the axial stress is removed.

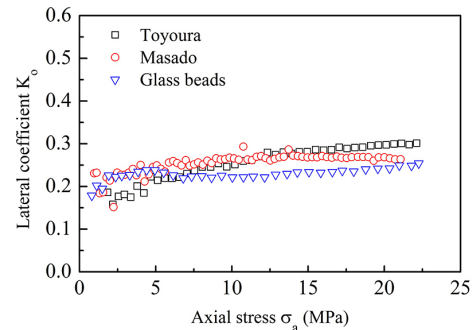


**Fig. 14.** Relationship between lateral earth pressure coefficient  $K_o$  and axial stress for three kinds of granular material during loading

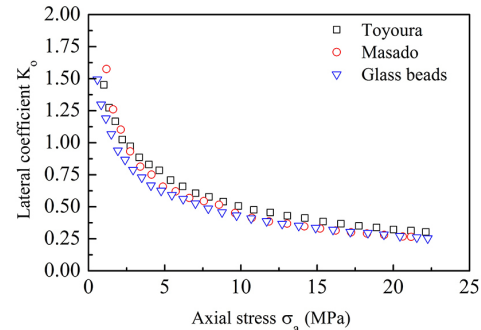


**Fig. 15.** Relationship between lateral earth pressure coefficient  $K_o$  and axial stress for three kinds of granular material during unloading

## 5 Confirmation of Degree of Particle Crushing

Confirmation of particle crushing occurrence and evaluation of grading curves are implemented by two common approaches in this study. One is to compare the GSD curves of each granular material before and after loading, the alternative is to make comparisons with the scanning electron microscopic photographs for the original and tested granular material.

To examine the effect of loading mode on the crushing degree of the same kind of granular material, the variation in the GSD curves of the granular material under one-dimensional and triaxial compression loadings are compared at almost the same mean stress level.

### 5.1 Grain size distribution curve before and after particle crushing occurrence

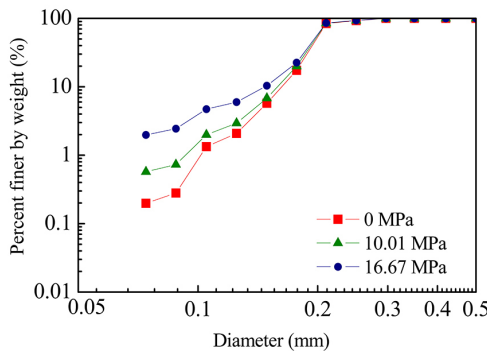
Figs. 16-18 show the GSD curves at the maximum axial stress of 0 MPa, 10.01 MPa and 16.67 MPa for Toyoura sand, Masado and glass beads ballotini, respectively. The axial stress here refers to the mean stress acted on the specimen. It is noted that the original curves shift to the left and upward as the applied axial stress increases. To quantitatively describe the degree of particle crushing, one simple breakage index  $B_{15}$  proposed by Lee & Farhoomand (1967) expressed as Eq. (2) is adopted in this study [35].

$$B_{15} = \frac{D_{15i}}{D_{15f}} \quad (2)$$

where  $D_{15i}$  and  $D_{15f}$  indicate the diameter in corresponding to the fine percent by weight as 15% for GSD curves at the initial and final state. Breakage index  $B_{15}$  is largest for Masado as 1.175. It is ascertained that crushability of Masado is higher than the other two granular materials.  $B_{15}$  is determined as 1.022 for glass beads ballotini which is slightly lower than that of Toyoura sand. Minor production of fines can be seen for glass beads ballotini. Table 3 shows the breakage index  $B_{15}$  for Toyoura sand, Masado and glass beads ballotini.

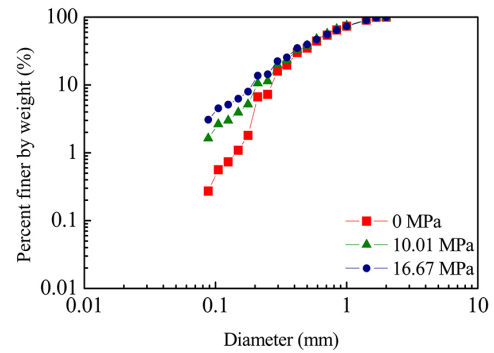
It is pointed out by Altuhafi and Coop (2011), Miao and Airey (2013) that the degree of particle crushing is greatly influenced by the loading mode and condition [36, 37]. Therefore, the effect of the loading mode on the degree of particle crushing is examined in this study. In contrast to the stress state in one-dimensional compression test, the radial stress is independent of the variation in the axial stress in triaxial compression test.

Fig. 19 compares both the grading distributed curves for Toyoura sand after one-dimensional compression and triaxial compression with the original one, respectively.



**Fig. 16.** Grain size distribution curves of Toyoura sand before and after loading

Owing to the limited triaxial test data demonstrating the change of GSD curves after shearing for Toyoura sand, the results of the experiment conducted by Miura (1971) with a mean stress of 11.7 MPa being acted on specimen is employed. It is clearly shown that the GSD curve after triaxial compression test markedly shifts left and upward although the mean stress applied is slightly higher than that in one-dimensional compres-



**Fig. 17.** Grain size distribution curves of Masado before and after loading

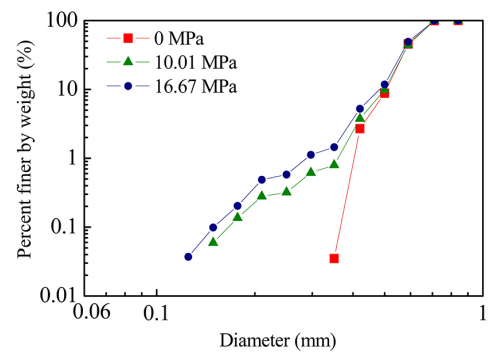


**Fig. 18.** Grain size distribution curves of glass beads ballotini before and after loading

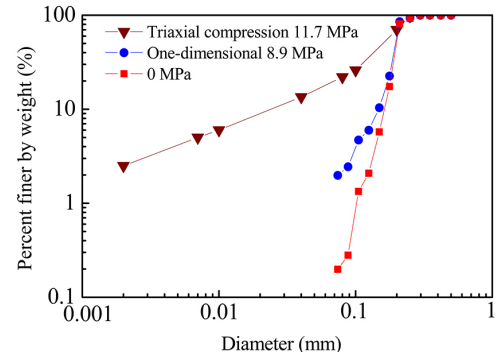


**Fig. 19.** Grain size distribution curves of Toyoura sand under triaxial compression and one-dimensional loadings

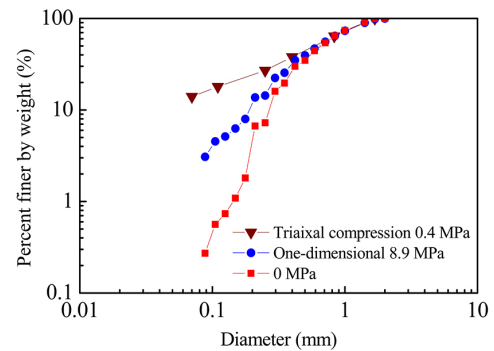


**Fig. 20.** Grain size distribution curves of Masado under triaxial compression and one-dimensional loadings

**Tab. 3.** Breakage index  $B_{15}$  of three granular materials under one-dimensional compression

Breakage index	Toyoura sand	Masado	Glass beads ballotini
$D_{15i}$ (mm)	0.172	0.295	0.512
$D_{15f}$ (mm)	0.158	0.251	0.501
$B_{15}$	1.089	1.175	1.022

sion test [2]. The breakage index  $B_{15}$  for Toyoura sand after triaxial compression testing is 3.731, almost three and a half times of that after one-dimensional compression test. However, the rate of the two corresponding mean stress levels for triaxial and one-dimensional compression test is just around 1.3.

Fig. 20 represents the grain size grading for Masado before and after testing, subjected to one-dimensional and triaxial loading [38]. The obvious shift of GSD curve is observed for Masado under triaxial test loading mode even though the mean stress on the specimen is only 0.4 MPa, which is much lower than that being applied in the one-dimensional tests. The breakage index  $B_{15}$  for Masado subjected to triaxial testing is 3.686. The difference in breakage index  $B_{15}$  during the triaxial loading mode is resulted as the existence of significant high shear stress within the specimen. The experimental results express a similar tendency with those reported by Miao and Airey (2013) [37]. The crushing degree in that test was more remarkable because the sand were tested until to the steady state. The breakage mechanisms for compression and shearing are basically distinct and produce different amounts of damage. The relative flow of particles subjected to shear stress increases the possibility of coordination numbers for particles.

## 5.2 Scanning electron microscopic photographs of granular material before and after loading

Figs. 21 - 23 represent the scanning electron microscopic photographs of Toyoura sand, Masado and glass beads ballotini before and after one-dimensional compression testing. The maximum magnification zoom lens of the scanning electron microscopic (SEM) is 500. Remarkable differences in appearance for the three granular materials are observed. In each figure, subtitle (a) shows the granular material before testing and (b) shows it after testing. The crushed granular material shown in (b) is the specimen taken from the cylinder cell after the sieving test to clearly identify the particle breakage of specimen.

Fig. 21(b) and Fig. 22(b) demonstrate that some individual particles experience significant crushing and fracturing and produce a large amount of fines. In comparison with Toyoura sand, the volume of fine content for Masado is relatively larger because that the single particle strength of Masado is lower [13, 39]. Masado is a typical sand composed of grains with different hardness. Low-hardness particles are crushed early on, intensifying the crushing degree as loading increases.

It is noted that glass beads ballotini displays different breakage pattern for individual grains compared with the other two natural sands. The individual ballotini separates into some small

irregular fragments. The breakage failure for natural sand generally starts from the edge of an individual particle. However, the breakage pattern of glass beads ballotini is conferred that the one crack appears on a single ballotini which subsequently decomposes into smaller parts. That breakage pattern is sufficient to explain why the axial strain of glass beads ballotini is smaller than that of Toyoura sand and Masado under the same axial stress level in Fig. 9.

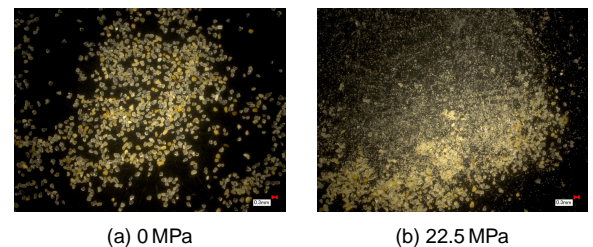


**Fig. 21.** SEM photographs of Toyoura sand before and after one-dimensional compression

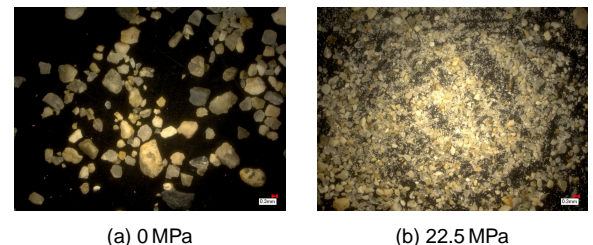


**Fig. 22.** SEM photographs of Masado before and after one-dimensional compression

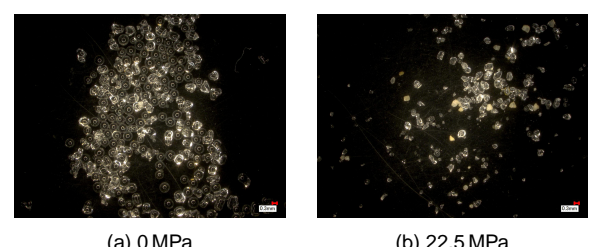


**Fig. 23.** SEM photographs of glass beads ballotini before and after one-dimensional compression

## 6 Conclusions

A series of one-dimensional high pressure compression tests was conducted on three granular materials in a dense state with different mineral composition and hardness. The strength and deformation characteristics of granular materials have been investigated under the maximum axial load terminated at 6 kN,

15 kN, 30 kN and 50 kN, respectively. Some major conclusions are made as follows:

- 1 A one-dimensional high pressure compression testing apparatus with the capacity of measuring the axial and lateral stresses acting on the cylindrical specimen simultaneously was developed.
- 2 The break-point stress identified from  $e - \log p$  curve was the largest for glass beads ballotini and smallest for Masado. The break-point stress is greatly dependent on the mineral composition and hardness of granular materials. The deformability and compressibility increase sharply once the axial stress exceeds the break-point stress for each granular material.
- 3 For the same granular material, the axial stress-strain curves express a similar shape and pattern in the four loading phases. The axial strain level for Masado is the largest at the maximum axial stress. Additionally, experimental results demonstrate that irrecoverable strain for Masado is the largest as well. The entire loading phase is divided into primary compression and secondary compression. The primary compression constrained modulus for glass beads ballotini is lower than that of the other two natural sands due to the difficulty of relative sliding and movement for glass beads ballotini. Conversely, the constrained modulus of the secondary compression phase for glass beads is high because almost no fines are produced during loading. Test results demonstrate that the constrained modulus during unloading is less dependent on the mineral composition of granular material.
- 4 The lateral earth pressure coefficient at rest  $K_o$  attains 0.2 at low axial stress and enters into a steady region with slight change as the axial load is increased.  $K_o$  at maximum axial stress level for Toyoura sand, Masado and glass beads are 0.29, 0.25 and 0.24, respectively. This difference mainly originates from the different frictional angles of the three granular materials. A rise in  $K_o$  is observed in tests for all three granular materials subjected to unloading.
- 5 The occurrence of particle crushing for three granular materials is confirmed by comparing the GSD curves before and after one-dimensional compression tests. The simple breakage index  $B_{15}$  is calculated for each granular material. Breakage index  $B_{15}$  is largest for Masado, at 1.175 among them. The effect of the loading mode on the degree of particle crushing for the same granular material is confirmed. The extensive crushing for specimens in triaxial testing is due to the existence of significantly high shear stress.
- 6 It is noted that the difference in breakage pattern for the natural sands and artificial glass beads ballotini is obviously identified from the SEM photographs after loading. The occurrence of breakage failure for natural sand usually starts from the edge of an individual particle and a large volume of fines is produced. However, the breakage pattern of glass beads

ballotini is conferred that the crack appears on a single ballotini which subsequently decomposes into small parts.

## References

- 1 **Vesic AS, Clough GW**, *Behavior of granular materials under high stresses*, Journal of Soil Mechanics and Foundations Div, **94**(3), (1968), 661–688, <http://cedb.asce.org/cgi/WWWdisplay.cgi?15488>.
- 2 **Miura N, Yamanouchi T**, *Drained shear characteristics of standard sand under high confining pressures*, Proceeding of the Japan of Society of Civil Engineers, **193**, (1971), 69–79, <http://library.jsce.or.jp/jsce/open/00037/191.html>.
- 3 **Miura N, Murata H, Yasufuku N**, *Stress-strain characteristics of sand in a particle-crushing region*, Soils and foundations, **24**(1), (1984), 77–89, DOI 10.3208/sandf1972.24.77.
- 4 **Hardin BO**, *Crushing of soil particles*, Journal of Geotechnical Engineering, **111**(10), (1985), 1177–1192, DOI 10.3208/sandf1972.24.77.
- 5 **Fukumoto T**, *Particle breakage characteristics of granular soils*, Soils and foundations, **32**(1), (1992), 26–40, DOI 10.3208/sandf1972.32.26.
- 6 **Lade PV, Yamamoto JA, Bopp PA**, *Significance of particle crushing in granular materials*, Journal of Geotechnical Engineering, **122**(4), (1996), 309–316, DOI 10.1061/(ASCE)0733-9410(1996)122:4(309).
- 7 **Yasufuku N, Hyde A**, *Pile end-bearing capacity in crushable sands*, Géotechnique, **45**(4), (1995), 663–676, DOI 10.1680/geot.1995.45.4.663.
- 8 **Kuwajima K, Hyodo M, Hyde AF**, *Pile bearing capacity factors and soil crushability*, Journal of geotechnical and geoenvironmental engineering, **135**(7), (2009), 901–913, DOI 10.1061/(ASCE)GT.1943-5606.0000057.
- 9 **Wu Y, Yamamoto H, Yao Y**, *Numerical study on bearing behavior of pile considering sand particle crushing*, Geomechanics and Engineering, **5**(3), (2013), 241–261, DOI 10.12989/gae.2013.5.3.241.
- 10 **Wu Y, Yamamoto H**, *Numerical Analysis of the Effect of Pile Tip Shape on Soil Behavior around Pile*, Geotechnical Engineering SEAGS & AGSSEA, **45**(2), (2014), 78–89.
- 11 **Hagerty MM, Hite DR, Ullrich CR, Hagerty DJ**, *One-dimensional high-pressure compression of granular media*, Journal of Geotechnical Engineering, **119**(1), (1993), 1–18, DOI 10.1061/(ASCE)0733-9410(1993)119:1(1).
- 12 **Nakata Y, Kato Y, Hyodo M, Hyde AFL, Murata H**, *One-Dimensional Compression Behaviour of Uniformly Graded Sand Related to Single Particle Crushing Strength*, Soils and foundations, **41**(2), (2001), 39–51, DOI 10.3208/sandf.41.2\_39.
- 13 **Nakata Y, Hyodo M, HYDE AFL, Kato Y, Murata H**, *Microscopic particle crushing of sand subjected to high pressure one-dimensional compression*, Soils and Foundations, **41**(1), (2001), 69–82, DOI 10.3208/sandf.41.2\_39.
- 14 **Graham J, Alfaro M, Ferris G**, *Compression and strength of dense sand at high pressures and elevated temperatures*, Canadian Geotechnical Journal, **41**(6), (2004), 1206–1212, DOI 10.1139/T04-047.
- 15 **Yamamoto JA, Bopp PA, Lade PV**, *One-dimensional compression of sands at high pressures*, Journal of Geotechnical Engineering, **122**(2), (1996), 147–154, DOI 10.1061/(ASCE)0733-9410(1996)122:2(147).
- 16 **Wang Z, Wong RCK**, *Effect of grain crushing on 1D compression and 1D creep behavior of sand at high stresses*, Geomechanics and Engineering, **2**(4), (2010), 303–319, DOI 10.12989/gae.2010.2.4.303.
- 17 **Mesri G, Hayat TM**, *The coefficient of earth pressure at rest*, Canadian Geotechnical Journal, **30**(4), (1993), 647–666, DOI 10.1139/t93-056.
- 18 **Vardhanabhoti B, Mesri G**, *Coefficient of earth pressure at rest for sands subjected to vibration*, Canadian Geotechnical Journal, **44**(10), (2007), 1242–1263, DOI 10.1139/T07-032.
- 19 **Mesri G, Vardhanabhoti B**, *Compression of granular materials*, Canadian Geotechnical Journal, **46**(4), (2009), 369–392, DOI 10.1139/T08-123.
- 20 **Northcutt S, Wijewickreme D**, *Effect of particle fabric on the coefficient of lateral earth pressure observed during one-dimensional compression of sand*,

Canadian Geotechnical Journal, **50**(5), (2013), 457–466, DOI 10.1139/cgj-2012-0162.

- 21 **McDowell GR, Bolton MD**, *On the micromechanics of crushable aggregates*, Géotechnique, **48**(5), (1998), 667–679, DOI 10.1680/geot.1998.48.5.667.
- 22 **McDowell GR, de Bono JP**, *On the micro mechanics of one-dimensional normal compression*, Géotechnique, **63**(11), (2013), 895–908, DOI 10.1680/geot.12.P.041.
- 23 **Minh NH, Cheng YP**, *One dimensional compression of gap-graded mixtures in DEM*, In: the International Symposium on Geomechanics and Geotechnics: From Micro to Macro; Shanghai, China, 2010, pp. 727–731.
- 24 **Ueda T, Matsushima T, Yamada Y**, *DEM simulation on the one-dimensional compression behavior of various shaped crushable granular materials*, Granular Matter, **15**(5), (2013), 675–684, DOI 10.1007/s10035-013-0457-1.
- 25 **Wang Y-H, Gao Y**, *Examining the behavior and mechanisms of structuration in sand under the K0 condition*, Granular matter, **16**(1), (2014), 55–68, DOI 10.1007/s10035-013-0457-1.
- 26 **Toyota H, Nakamura K, Kazama M**, *Shear and liquefaction characteristics of sandy soils in triaxial tests*, Soils and foundations, **44**(2), (2004), 117–126, DOI 10.3208/sandf.44.2\_117.
- 27 **Tsuchida T, Athapaththu RG, Kano S, Suga K**, *Evaluation of In-Situ Shear Strength of Natural Slopes Vulnerable to Heavy Rainfall by Lightweight Dynamic Cone Penetrometer*, the 2nd International Conference GEDMAR08, In:, Nanjing, China, 2008, pp. 578–584, DOI 10.1007/978-3-540-79846-0\_70.
- 28 **Kumruzzaman M, Yin J-H**, *Stress-Strain Behaviour of Completely Decomposed Granite in Both Triaxial and Plane Strain Conditions*, Jordan Journal of Civil Engineering, **6**(1), (2012).
- 29 **Hendron AJ**, *The behavior of sand in one-dimensional compression*, PhD thesis, University of Illinois at Urbana-Champaign; Illinois, USA, 1963.
- 30 **Roberts J**, *Sand compressibility as a factor in oil field subsidence*, PhD thesis, Massachusetts Institute of Technology; Cambridge, USA, 1965.
- 31 **Einav I**, *Breakage mechanics—part I: theory*, Journal of the Mechanics and Physics of Solids, **55**(6), (2007), 1274–1297, DOI 10.1016/j.jmps.2006.11.003.
- 32 **Mesri G**, *Primary compression and secondary compression*, Geotechnical Special Publication, **11**, (2003), 122–166, DOI 10.1061/40659(2003)5.
- 33 **Bishop AW**, *Test requirements for measuring the coefficient of earth pressure at rest*, In: Brussels Conference earth Pressure Problem; Brussels, 1958, pp. 2–14.
- 34 **Gao Y, Wang YH**, *Experimental and DEM Examinations of K 0 in Sand under Different Loading Conditions*, Journal of Geotechnical and Geoenvironmental Engineering, **140**(5), (2014), 04014012, DOI 10.1061/(ASCE)GT.1943-5606.0001095.
- 35 **Lee KL, Farhoomand I**, *Compressibility and crushing of granular soil in anisotropic triaxial compression*, Canadian Geotechnical Journal, **4**(1), (1967), 68–86, DOI 10.1139/t67-012.
- 36 **Altuhafi FN, Coop MR**, *The effect of mode of loading on particle-scale damage*, Soils and foundations, **51**(5), (2011), 849–856, DOI 10.3208/sandf.51.849.
- 37 **Miao G, Airey D**, *Breakage and ultimate states for a carbonate sand*, Géotechnique, **63**(14), (2013), 1221–1229, DOI 10.1680/geot.12.P.111.
- 38 **Murata H, Hyodo M, Yasufuku N**, *Prediction of Stress–Strain Behaviour of Undisturbed “Masado”*, Technology reports of the Yamaguchi University, **4**(2), (1988), 161–170.
- 39 **Wu Y, Yamamoto H**, *Numerical investigation on the reference crushing stress of granular materials in triaxial compression test*, Periodica Polytechnica Civil Engineering, **59**, (2015), DOI 10.3311/PPci.7694.